

# Solubility of carbon dioxide (CO<sub>2</sub>) in aqueous solution of 3-(dimethylamino)-1-propylamine (DMAPA)

Devjyoti Nath, Amr Henni<sup>\*</sup>

Acid Gas Removal Laboratory, Clean Energy Technologies Research Institute (CETri), University of Regina, Regina, SK, Canada

## ARTICLE INFO

### Article history:

Received 29 October 2019

Received in revised form

20 December 2019

Accepted 31 January 2020

Available online 4 February 2020

### Keywords:

Solubility

Carbon dioxide

3-(Dimethylamino)-1-propylamine

Electrolyte-NRTL model

## ABSTRACT

The main objective of this study is to investigate the efficiency of 3-(Dimethylamino)-1-propylamine (DMAPA) as a solvent for carbon dioxide (CO<sub>2</sub>) capture. The solubility of CO<sub>2</sub> in aqueous solutions of DMAPA was measured at (313.15 and 333.15) K and at a partial pressure of CO<sub>2</sub> up to 275 kPa using the pressure-decay method. Measurements were performed at two concentrations of DMAPA (15 wt % and 30 wt %). DMAPA exhibited high CO<sub>2</sub> loading when compared with other benchmark amines for CO<sub>2</sub> absorption technology such as mono-ethanolamine (MEA) and piperazine (PZ). In this study, the highest CO<sub>2</sub> loading recorded was 1.46 at 313.15 K at a CO<sub>2</sub> partial pressure of 271 kPa. The experimental solubility data were correlated with the electrolyte-NRTL model, and the Redlich-Kwong (RK) equation of state was used for the estimation of the vapor phase fugacity coefficients at equilibrium. Excess enthalpy ( $H^E$ ) for DMAPA-water binary system was measured using a C80 flow calorimeter at (313.15 and 333.15) K. Binary NRTL parameters for DMAPA/H<sub>2</sub>O were regressed from the excess enthalpy ( $H^E$ ) data of the DMAPA-water system; and some other parameters such as the molecule-ion pair parameters, equilibrium constants, etc. were regressed using vapor-liquid equilibrium (VLE) data. Finally, the Gibbs-Helmholtz equation was used to predict the heat of absorption of CO<sub>2</sub> solubility in the amine solution based on solubility data.

© 2020 Elsevier B.V. All rights reserved.

## 1. Introduction

More than 80% of energy is generated by burning fossil fuels. Unfortunately, this process is accelerating global warming by emitting large amounts of CO<sub>2</sub> into the atmosphere. In 2016, emissions set a new record of about 1.1 °C above the pre-industrial period. According to a report by the World Meteorological Organization (WMO) in 2019 [1], the annual mean concentration of CO<sub>2</sub> in 2018 was 408 ppm (about 2 ppm higher than the concentration in 2017), and the arctic sea-ice extent reached its lowest level ever in July 2019. Therefore, the capture of CO<sub>2</sub> from flue gases has become crucial to protect the environment. One of the most technologically advanced methods to capture CO<sub>2</sub> for mitigating emissions from large stationary point sources is its absorption by liquid solvent, mainly mixtures of amines. One of the major challenges of this research is to find a cost-effective and environmentally friendly liquid solvent. It is a great challenge to come up with a commercially successful solvent, as many liquid solvents have already been

proposed by different researchers to capture CO<sub>2</sub> from flue gas. However, all solvents have their own benefits and demerits.

Although CO<sub>2</sub> capture with amine-based solvent is one of the most common and advanced technologies available nowadays for post-combustion CO<sub>2</sub> capture, this technology is still not economically viable due to high regeneration cost, high solvent degradation rate and high corrosivity of amine-base solvent. Therefore, a major research challenge nowadays in investigating CO<sub>2</sub> absorption is to find an environmentally friendly liquid solvent taking these concerns into account. Several amines have already been tested as potential solvents for CO<sub>2</sub> capture, but all the amine-based solvents have demonstrated advantages and disadvantages. For example, monoethanolamine (MEA) demonstrated decent CO<sub>2</sub> loading (amount of CO<sub>2</sub> absorbed in amine), high kinetics (absorption rate), etc. but it also demonstrated high degradation rate and caused corrosion problems. Another common amine, methyldiethanolamine (MDEA), demonstrated a higher capacity to absorb CO<sub>2</sub> but it showed poor kinetics rates. Piperazine (PZ), a diamine with two secondary amino groups in its structure, demonstrated better performance for CO<sub>2</sub> capture when compared to MEA and MDEA in terms of reaction rate, thermal and oxidative stability and CO<sub>2</sub>

<sup>\*</sup> Corresponding author.

E-mail address: [amr.henni@uregina.ca](mailto:amr.henni@uregina.ca) (A. Henni).

loading [2], but PZ is not highly soluble in water, and therefore, there is high possibility of precipitation of PZ during absorption/stripping [3]. There was also a chance of the formation of nitrosamine (NNO) which is one of the most carcinogenic by-products by the reaction of  $\text{NO}_2$  in the flue gas with piperazine solvent [4]. Even though piperazine demonstrated a high potential as a solvent for  $\text{CO}_2$  capture but it cannot be used as a standalone solvent in post-combustion  $\text{CO}_2$  capture, and several piperazine derivatives such as 1-methylpiperazine and 2-methylpiperazine have therefore been tested by a number of researchers [2,5]. These piperazine based derivatives demonstrated high cyclic  $\text{CO}_2$  capacity, however, they exhibited lower reaction rate compared to piperazine [6].

Simulation is the most common and effective way of optimizing the process design and operations of  $\text{CO}_2$  capture technology [7]. A proper thermodynamic model is essential for an effective process simulation. The developed thermodynamic model will use the experimental results to provide the opportunity to predict the performance of an amine solvent at different operating conditions. It is important to note that experimental results acquired over a wide range of temperatures and pressures are necessary to develop such a model.

Several thermodynamic models have been used to model vapor-liquid equilibrium (VLE) data of  $\text{CO}_2$ -amine-water system. Klyamer et al. (1973) first modeled the vapor-liquid equilibrium (VLE) data of  $\text{CO}_2$ -ethanolamine-water system [8], and the activity coefficients of the species present in the liquid phase were estimated using Debye-Hückel limiting law. Kent and Eisenberg correlated VLE data of  $\text{CO}_2$ -amine-water system by setting the activity coefficient models to unity [8]. A rigorous activity coefficient based model was proposed by Deshmukh and Mather to model several VLE data of  $\text{CO}_2$ -amine-water systems. In this model, the Debye-Hückel limiting law was used to estimate the activity coefficient of the species present in the liquid phase, the Peng-Robinson equation of state (EOS) was employed to estimate the vapor phase fugacity coefficient, and all the equilibrium constants were taken from the previously published articles. Later, Chen and Evans proposed an excess Gibbs energy based model, the electrolyte-NRTL (elec-NRTL) model [9]. They used the Pitzer-Debye-Hückel equation to predict the long-range interactions and reformulated the NRTL equation for electrolytes to predict the short-range interactions. The electrolyte-NRTL model is considered as the most rigorous and is a widely used model for electrolyte systems nowadays.

Due to the high regeneration cost, higher rate of solvent degradation and corrosiveness of all commercially available solvents till now, investigations are still underway to find better amine solvent for post-combustion  $\text{CO}_2$  capture. A recent amine screening study suggested a number of new amines for  $\text{CO}_2$  capture from the flue gas [10]. In a more recent study reported by El Hadri et al. [11], 3-(dimethylamino)-1-propylamine (DMPA) was shown to have a great potential as a solvent of  $\text{CO}_2$  capture; and thereafter in 2018, the solubility of  $\text{CO}_2$  in 2M aqueous DMPA at 313.15 K and at a limited range of  $\text{CO}_2$  partial pressures less than 101 kPa has been published in a different study [12]. DMPA is a diamine with a primary and a tertiary amino group in its structure. Cachaza et al. (2018) studied the absorption rate and cyclic capacity of  $\text{CO}_2$  in DMPA [13], and mentioned that 3-dimethylamino-propylamine can be considered an appropriate amine to industrial carbon dioxide absorption process.

The main objective of this present study is to investigate further the solubility of  $\text{CO}_2$  in DMPA at different operating conditions (a wider range of temperatures and pressures). The solubility of  $\text{CO}_2$  in aqueous diamine, 3-(dimethylamino)-1-propylamine (DMPA), was measured at (313.15 and 333.15) K and at partial pressures of  $\text{CO}_2$  up to 300 kPa using the pressure-decay method in a stirred cell reactor. In the present study,  $\text{CO}_2$  solubility was measured at two

different concentrations of DMPA (15 wt % and 30 wt %) of industrial relevance at both temperatures. DMPA exhibited high  $\text{CO}_2$  loading compared with the other benchmark amines for  $\text{CO}_2$  absorption such as MEA and piperazine. DMPA exhibited about 1.35 and 1.94 times more  $\text{CO}_2$  loading capacity at the same temperature (313.15 K) and pressure (271 kPa) compared to piperazine and MEA, respectively. Based on this study, DMPA can be considered a promising solvent for carbon capture from natural and flue gases. Finally, the experimental solubility data were correlated with the electrolyte-NRTL model, and the Redlich-Kwong (RK) equation of state was used for estimation of vapor phase fugacity coefficient of the equilibrium. The model was developed in two stages: (i) binary NRTL parameters for DMPA/ $\text{H}_2\text{O}$  were regressed from the excess enthalpy ( $H^E$ ) data of the DMPA-water system in first steps, and (ii) the elec-NRTL parameters (molecule-ion pair parameters) and equilibrium constants were regressed from the experimental data of  $\text{CO}_2$  solubility in aqueous DMPA. Excess enthalpies for the DMPA-water binary system were measured using C80 Setaram flow calorimeter at (313.15 and 333.15) K. Gibbs-Helmholtz equation was used to estimate the heat of absorption of  $\text{CO}_2$  solubility in amine from the solubility data.

## 2. Experimental methodology

### 2.1. Materials

3-(Dimethylamino)-1-propylamine (DMPA) and mono-ethanolamine (MEA) were purchased from Sigma-Aldrich and used without further purification. Carbon dioxide was purchased from Praxair. The structures, suppliers, purities and water contents of all the chemicals used in the present study are listed in Table 1.

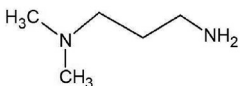

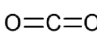
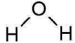
### 2.2. Measurement of $\text{CO}_2$ solubility

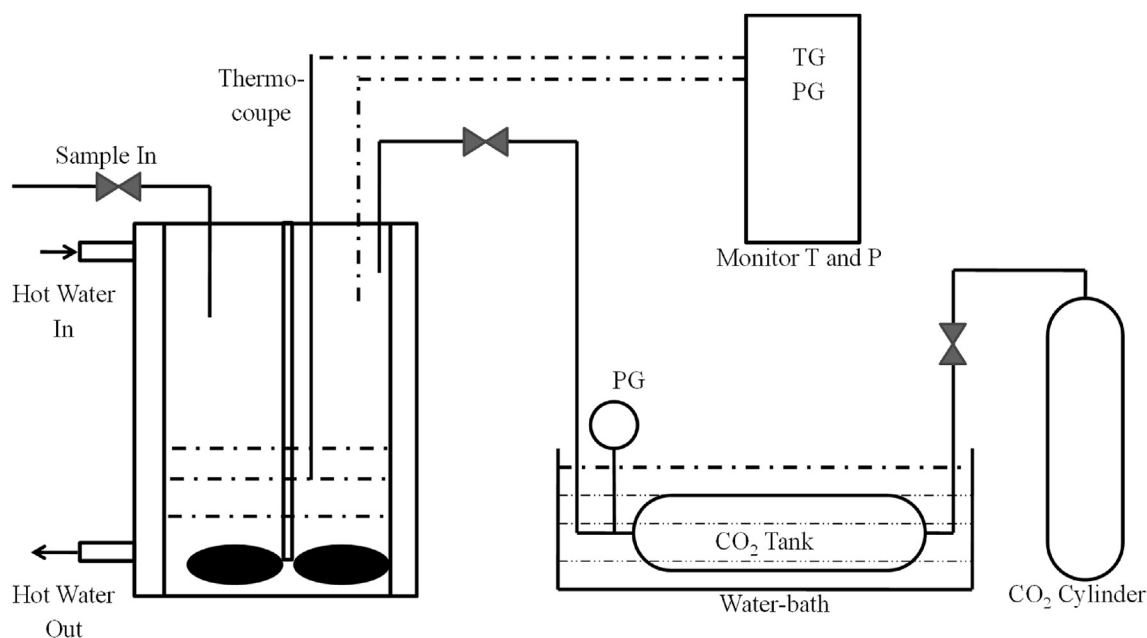
The schematic diagram of the experimental setup that used in this study is shown in Fig. 1. This experimental setup contains a stirred cell reactor and a stainless steel gas reservoir. A 1 L stirred cell glass reactor from Autoclave Engineers was used in this study to measure the  $\text{CO}_2$  solubility in the aqueous phase. One motor-driven mechanical stirrer was attached to the reactor to mix the  $\text{CO}_2$  into the aqueous solvent and therefore reduce the time to reach equilibrium conditions. A K-type thermocouple with an uncertainty of 0.5 K and a pressure transmitter with an uncertainty of 0.89 kPa were connected to the reactor. The reactor temperature was maintained by flowing hot water through the water jacket of the reactor from a water bath. A 300 ml stainless steel gas reservoir was submerged into another hot water bath to preheat the gas up to the reaction condition. The pressure of the gas reservoir was measured by a pressure gauge with an accuracy of  $\pm 0.25$  % of full-scale (FS). To ensure the temperature of the water bath, Ertco-Hart RTD digital thermometer (model 850C) with the uncertainty of 0.01 K was used.

Pressure decay method was used to measure the solubility of  $\text{CO}_2$  in aqueous amine solution and a similar method was also used in various literatures to perform the experiment on vapor-liquid equilibrium [14,15]. In this study, the actual volume of the reactor was measured to reduce the experimental error. The solubility of the  $\text{CO}_2$  was measured at 313.15 K and 333.15 K. Before starting the solubility experiment, the reactor was flashed with  $\text{N}_2$  three times to ensure that there was no oxygen left inside the reactor, then a known volume of aqueous solvent was transferred into the reactor and the stirrer was turned on to raise the temperature of the liquid sample up to the required experimental condition. Once the temperature of the liquid sample reached the desired temperature, the sample was kept inside the reactor for another 4 h before

**Table 1**

Structure, abbreviation, supplier and purity of the chemicals used in this present study.

| Compound                        | Structure   | IUPAC names (Abbreviation)               | Source and Purity                    |
|---------------------------------|---|--|--------------------------------------|
| 3-(Dimethylamino)-1-propylamine |  | N,N'-dimethylpropane-1,3-diamine (DMAPA) | Sigma-Aldrich (99 wt%) <sup>a</sup>  |
| Monoethanolamine                |  | 2-aminoethanol (MEA)                     | Sigma-Aldrich (≥98 wt%) <sup>a</sup> |
| Carbon dioxide                  |  | Carbon dioxide (CO <sub>2</sub> )        | Praxair (99.995 vol%) <sup>a</sup>   |
| Distilled Water                 |  | Water (H <sub>2</sub> O)                 | Prepared in the lab                  |

<sup>a</sup> Provided by supplier.**Fig. 1.** Schematic diagram of the experimental set-up.

introducing the CO<sub>2</sub> to make sure all amine-water system reached thermal equilibrium. When the pressure was stable, its value was recorded. On the other hand, CO<sub>2</sub> was preheated inside the reactor for about 2 h and the pressure of the CO<sub>2</sub> was recorded. Then the valve between the reactor and the CO<sub>2</sub> vessel was opened to transfer the CO<sub>2</sub> inside the reactor. When the pressure of the reactor and vessel became equal, the valve was turned off. The temperature of the vessel might have changed due to the pressure change; therefore, the pressure reading of the vessel was taken after 10–15 min so that the temperature of the vessel reached back to the desired temperature. The amount of CO<sub>2</sub> transferred into the reactor was estimated with the gas law based on the pressure and temperature readings at the beginning and the end of the CO<sub>2</sub> transfer (Eq. (1)).

$$n_{\text{CO}_2} = \frac{P_i V_g}{RTZ_i} - \frac{P_f V_g}{RTZ_f} \quad (1)$$

where,  $n_{\text{CO}_2}$  represents the number of moles of CO<sub>2</sub> transferred into the reactor,  $P_i$  and  $P_f$  represent the pressure at the beginning and the end of CO<sub>2</sub> transfer.  $V_g$ ,  $R$ ,  $T$  and  $Z_i$  are the volume of the vessel, the gas constant, the operating temperature and compressibility

factor of CO<sub>2</sub>, respectively.

When the CO<sub>2</sub> transfer to the reactor was completed, the valve between the reactor and gas vessel was turned off to the close position. The stirrer was then turned on at 100 rpm speed and equilibrium was reached after about 8 h. The pressure inside the reactor was recorded if it stayed constant for at least 1 h. The amount of CO<sub>2</sub> in the gas phase was estimated from the real gas law, and the amount of CO<sub>2</sub> absorbed was estimated from the difference between the CO<sub>2</sub> transferred to the reactor and the rest of CO<sub>2</sub> that existed in the gas phase.

### 2.3. Measurement of excess enthalpy

The excess enthalpies ( $H^E$ ) for the DMAPA-water binary system were estimated using a C80 flow calorimeter at (313.15 and 333.15) K by following the experimental methodology published by Mathonat et al. (1994) [16]. A mixing flow unit (manufactured for us by Setaram Instrument, France) integrated into a C-80 calorimeter (Setaram Instrument, France) was used to measure the excess enthalpy. Details about the experimental set-up were published by Rayet and Henni (2014) [17]. The mixing unit is connected to two ISCO (Model 100 DM) high-pressure syringe pumps in order to feed

the water and the amine to the mixing unit at a selected flow rate. These syringe pumps can maintain a stable flow rate with a relative uncertainty of 0.2%. The flow rates were varied in between (0.1 and 0.5) mL·min<sup>-1</sup> for maintaining the mole-fraction of amine and water at the experimental conditions. The pressure of the system was maintained at constant pressure with an uncertainty of 0.05 MPa using a Swagelok stainless steel back-pressure regulator (model type KPB1P0D412P2000) that was placed at the end of the flow line. The pressure was measured by three electronic Keller-pressure gauges (LEO1/300 bar/81002C) with an accuracy of 0.25%. Fluids were preheated at the set temperature with a Julabo Model F25 water bath (±1 K). Temperatures of the fluids were maintained at the correct temperature with preheaters to within 0.05 K.

At first, one fluid was fed to the mixing unit using one ISCO pump. When the base-line signal for the first liquid flowing through the calorimeter was well stabilized for 20–30 min, the second pump was turned-on to feed the second fluid into the mixing unit. The signal for the mixing of two liquids started to increase and reached the 'plateau'. The 'plateau' signal which corresponds to the actual mixing effect was achieved within 30 min after starting the mixing process. When the 'plateau' signal was well established for 40–60 min, one pump was turned off to stop introducing the fluid; allowing the signal to come back to the base-line value. The values of the Excess enthalpies ( $H^E$ ) were estimated using Eq. (2).

$$H^E = \frac{S_M - S_B}{n} \quad (2)$$

where,  $S_M$ ,  $S_B$  and  $n$  represent the 'plateau' signal (mW), base-line signal (mW) and total molar flow-rate of the mixture (mol·s<sup>-1</sup>), respectively.

#### 2.4. Verification of solubility data measurement

Two isotherm experiments were performed at 313.15 K to estimate the solubility of CO<sub>2</sub> in 15 wt % of aqueous MEA and a comparison was done with the results from several literature studies. The comparison between the results is shown in the form of P-x plots in Fig. 2 (solubility data are reported in Table S1 in supplementary information). In the present study, the estimated solubility data for CO<sub>2</sub> in 15 wt % MEA were found to be in good agreement with those published in the literature at low pressures (less than 3% AAD).

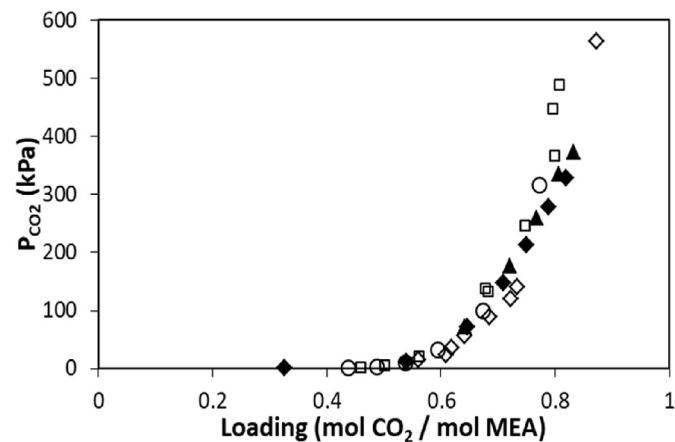
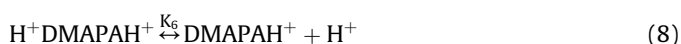
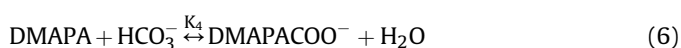


Fig. 2. Solubility data of CO<sub>2</sub> in 15 wt% of MEA at the temperature 313.15 K was compared with the literature. ▲: Run 1 (this study) and ◆: Run 2 (this study), ◇: Shen and Li [18], □: Lee et al. [19], and ○: Lee et al. [20].

### 3. Model

#### 3.1. Chemical reaction and equilibrium

3-(Dimethylamino)-1-propylamine (DMAPA) is a diamine with a primary and a tertiary amino group in its structure. The primary amino group can either be protonated (DMAPAH<sup>+</sup>) or reacts with CO<sub>2</sub> to form carbamate (DMAPACOO<sup>-</sup>). Again, the tertiary amino group of the protonated amine (DMAPAH<sup>+</sup>) or carbamate (DMAPACOO<sup>-</sup>) can also be protonated. Tissier and Barillier (1969) reported the first and second dissociation constant values [21]. The reactions mentioned below are considered to happen and are included in the thermodynamic model.



Chemical equilibrium can be expressed by the activity of the reactants and products, and the equilibrium constants of the above-mentioned reactions can be expressed by Eq. (10) [5].

$$\ln K_j = \sum_i \nu_{ij} \ln(a_i) = \sum_i \nu_{ij} \ln(x_i \gamma_i) \quad (10)$$

where,  $K_j$  represents the equilibrium constant of  $j$  reaction,  $\nu_{ij}$  represents the reaction stoichiometric coefficient of component  $i$  in  $j$  reaction, and  $a_i$ ,  $x_i$  &  $\gamma_i$  represent the activity, mole-fraction and activity coefficient of component  $i$ , respectively.

The standard state convention was applied for normalization to specify the reference state. The symmetric convention was applied when water and DMAPA are represented as the solvent in the liquid phase, and the activity coefficient of solvent (water or DMAPA) became the unity when the mole fraction is close to unity [2].

$$\gamma_s \rightarrow 1 \text{ when } x_s \rightarrow 1$$

Infinite dilution was defined as the reference state for the other molecular solutes and ions in the aqueous phase at temperature and pressure of the mixture [2]. HDMAPACOO was treated as the non-volatile Henry's components in the liquid phase [2].

$$\gamma^* \rightarrow 1 \text{ when } x_i \rightarrow 0$$

The equilibrium constants of the above-mentioned reactions can be expressed as temperature dependent function shown in Eq. (11). Coefficients of this function for various equilibrium constants are given in Table 2.

$$\ln K = A + \frac{B}{T} + C \ln T + DT \quad (11)$$

Equilibrium constants of Eqs. (7) and (8) were estimated from the data of dissociation constant of DMAPA provided by Tissier and Barillier (1969) [21]. Mole fraction base equilibrium ( $K_x^*$ ) constant was estimated from molality base asymmetric equilibrium constant

**Table 2**

Coefficients in temperature dependent function of equilibrium constants.

|                | A        | B         | C        | D | T       | Source                 |
|----------------|----------|-----------|----------|---|---------|------------------------|
| K <sub>1</sub> | 132.899  | −13445    | −22.4773 | 0 | −       | Aspen Data Bank        |
| K <sub>2</sub> | 231.465  | −12092.1  | −36.7816 | 0 | −       | Aspen Data Bank        |
| K <sub>3</sub> | 216.05   | −12431.7  | −35.4819 | 0 | −       | Aspen Data Bank        |
| K <sub>4</sub> | 114.734  | 5459.51   | −21.8464 | 0 | 313–333 | This work <sup>b</sup> |
| K <sub>5</sub> | 9.63165  | −11261.95 | 0        | 0 | 288–318 | This work <sup>a</sup> |
| K <sub>6</sub> | 11.7466  | −10322.43 | 0        | 0 | 288–318 | This work <sup>a</sup> |
| K <sub>7</sub> | −216.241 | 3478.72   | 31.1114  | 0 | 313–333 | This work <sup>b</sup> |

<sup>a</sup> Regressed with data from Tissier and Barillier (1969) [21].<sup>b</sup> Regressed at this work.(K<sub>m</sub><sup>\*</sup>) with Eq. (12) [22,23].

$$\ln K_x^* = \ln K_m^* + \ln \left( \frac{MW_w}{1000} \right) \sum_{i \neq w} v_i + \ln \gamma_{\text{amine}}^{\infty} \quad (12)$$

where, MW<sub>w</sub> is the molecular weight of water, and v<sub>i</sub> is the stoichiometric coefficient of the reaction.

### 3.2. Vapor phase equilibria

In this work, the Redlich-Kwong (RK) equation of state (EOS) was used for the vapor phase equilibria. At equilibrium, the liquid phase fugacity for each component is equal to the vapor phase fugacity. Vapor-liquid equilibrium of CO<sub>2</sub> can be represented with Eq. (13) associated with physical solubility (Henry's Law) and vapor-liquid equilibrium of the solvent species can be presented with Eq. (14), where, ϕ<sup>v</sup> is the fugacity coefficient of species in the vapor phase.

$$\phi^v y_i P = x_i \gamma_i^* H_i \exp \left( \frac{v_i^{\infty} (P - P_{\text{sol}}^0)}{RT} \right) \text{ where, } i = \text{CO}_2 \quad (13)$$

$$\phi^v y_i P = x_i \gamma_i P_i^0 \exp \left( \frac{v_i (P - P_i^0)}{RT} \right) \text{ where } i = \text{DMAP or H}_2\text{O} \quad (14)$$

Fugacity coefficient (ϕ<sup>v</sup>) at the vapor phase was estimated with Redlich-Kwong (RK) equation of state (EOS) which is given at Eq. (15) [24,25].

$$P = \frac{RT}{v_m - b} - \frac{a/T^{0.5}}{v_m(v_m + b)} \quad (15)$$

where,  $a_i = 0.4278 \frac{R^2 T_{ci}^{2.5}}{P_{ci}}$ ,  $b_i = 0.0867 \frac{RT_{ci}}{P_{ci}}$ , T<sub>ci</sub> and P<sub>ci</sub> are the critical temperature and pressure of the component i, respectively.

### 3.3. Electrolyte-NRTL model

In this work, the electrolyte-NRTL (elec-NRTL) was used for the liquid phase equilibria [5,7,23,26]. The electrolyte-NRTL, an activity coefficient based model, was used to estimate the excess Gibbs free energy by considering three types of contribution as shown in Eq. (16). The first contribution is the ion-ion long-range interaction due to the electrostatic force among all the ions, and this contribution is estimated with the Pitzer-Debye-Hückel formulation (PDH) [7,26]. Second contribution which is the ion-reference-state-transfer contribution is estimated with Born formulation by accounting the change in reference state for mixed solvent [7,26]. The last contribution is the local contribution which accounts for ion-ion short-range interaction [7,26], and this contribution is estimated with NRTL formulation.

$$\frac{G^E}{RT} = \frac{G^{E,PDH}}{RT} + \frac{G^{E,Born}}{RT} + \frac{G^{E,lc}}{RT} \quad (16)$$

The Pitzer-Debye-Hückel formulation to estimate the long-range ion-ion interaction which is shown in Eq. (17) is a function of molecular weight (M<sub>s</sub>), the Debye-Hückel parameter (A<sub>φ</sub>), the charge of the components (Z<sub>i</sub>), the 'closest approach parameter' (ρ) and the ionic strength (I<sub>x</sub>) [5,23]. The ionic strength (I<sub>x</sub>) and the Debye-Hückel parameter (A<sub>φ</sub>) are estimated with Eqs. (18) and (19), respectively.

$$\ln \gamma_i^{PDH} = \left( \frac{1000}{M_s} \right)^{1/2} A_{\phi} \left[ \left( \frac{2Z_i^2}{\rho} \right) \ln \left( 1 + \rho I_x^{1/2} \right) + \frac{Z_i^2 I_x^{1/2}}{1 + \rho I_x^{1/2}} \right] \quad (17)$$

$$I_x = \frac{1}{2} \sum_i x_i Z_i^2 \quad (18)$$

$$A_{\phi} = \frac{1}{3} \left( \frac{2\pi N_A d_s}{1000} \right)^{1/2} \left( \frac{Q_e^2}{\epsilon_w kT} \right)^{3/2} \quad (19)$$

where, N<sub>A</sub>, d<sub>s</sub>, Q<sub>e</sub>, ε<sub>w</sub> and k are the Avogadro's number, solvent density, charge of electron, the dielectric constant for water and Boltzmann constant, respectively.

Born correction was used to adjust the activity coefficient by accounting for the change in the reference state of mixed solvent as shown in Eq. (20).

$$\ln \gamma_i^{Born} = \frac{G^{*E,Born}}{RT} = \frac{Q_e^2}{2kT} \left( \frac{1}{\epsilon_m} - \frac{1}{\epsilon_w} \right) \frac{\sum_i x_i Z_i^2}{r_i} 10^{-2} \quad (20)$$

where, ε<sub>m</sub>, ε<sub>w</sub> and r<sub>i</sub> are the dielectric constant of the mixed solvent, dielectric constant of the water and Born radius. Dielectric constant of a mixed solvent can be estimated from the pure-component dielectric constant. Dielectric constant of pure component (B) shown in Eq. (21) is temperature dependent function, and dielectric constant of mixed solvent can be estimated by using Eq. (22).

$$\epsilon_B(T) = A_B + B_B \left[ \frac{1}{T} - \frac{1}{C_B} \right] \quad (21)$$

$$\epsilon_m = \sum_i w_{mi}^{sf} D_i \quad (22)$$

where, w<sub>mi</sub><sup>sf</sup> is the solute free mass fraction, and D<sub>i</sub> is the pure component dielectric constant.

NRTL formulation shown in Eq. (23) is used to estimate excess Gibbs energy accounted for short-range interaction among the species [7].

$$\begin{aligned} \frac{G_m^{*E,lc}}{RT} = & \sum_m X_m \sum_k X_k G_{km} \tau_{jm} + \sum_c X_c \sum_{a'} \left( \frac{X_{a'}}{\sum_{a''} X_{a''}} \right) \frac{\sum_j X_j G_{jc,a'c} \tau_{jc,a'c}}{\sum_k X_k G_{kc,a'c}} \\ & + \sum_a X_a \sum_{c'} \left( \frac{X_{c'}}{\sum_{c''} X_{c''}} \right) \frac{\sum_j X_j G_{ja,a'c} \tau_{ja,a'c}}{\sum_k X_k G_{ka,a'c}} \end{aligned} \quad (23)$$

$$\begin{aligned} \text{where, } G_{jm} = & \exp(-\alpha_{jm} \tau_{jm}), \quad G_{jc,ca} = \exp(-\alpha_{jc,ca} \tau_{jc,ca}), \\ G_{jc,ac} = & \exp(-\alpha_{jc,ac} \tau_{jc,ac}), \quad G_{cm} = \frac{\sum_a X_a G_{ca,m}}{\sum_{a'} X_{a'}}, \quad G_{am} = \frac{\sum_c X_c G_{ca,m}}{\sum_{c'} X_{c'}}, \\ \alpha_{mc} = & \alpha_{cm} = \frac{\sum_a X_a \alpha_{m,ca}}{\sum_{a'} X_{a'}}, \quad \alpha_{ma} = \alpha_{am} = \frac{\sum_c X_c \alpha_{m,ca}}{\sum_{c'} X_{c'}} \end{aligned}$$



**Table 3**  
Physical properties of the components used in this work.

| Properties                                  | CO <sub>2</sub> | H <sub>2</sub> O | DMAPA    | Source         |
|---|-----------------|------------------|----------|----------------|
| <i>T<sub>c</sub></i> (K)                    | 304.2           | 647.30           | 593.3    | Aspen database |
| <i>P<sub>c</sub></i> (kPa)                  | 7376.46         | 22048.3          | 3586     | Aspen database |
| <i>V<sub>c</sub></i> (m <sup>3</sup> /kmol) | 0.0939446       | 0.0558953        | 0.369    | Aspen database |
| <i>V<sub>B</sub></i> (m <sup>3</sup> /kmol) | 0.0356374       | 0.0196361        | 0.143238 | Aspen database |
| <i>ω</i>                                    | 0.225           | 0.344            | 0.4544   | Aspen database |
| <i>Z<sup>RA</sup></i>                       | 0.273615        | 0.243172         | 0.26792  | Aspen database |
| <i>T<sub>freezpt</sub></i> (K)              | 216.6           | 273.2            | 194.442  | Aspen database |

$$\tau_{ma,ca} = \tau_{am} - \tau_{ca,m} + \tau_{m,ca} \text{ and } \tau_{mc,ac} = \tau_{cm} - \tau_{ca,m} + \tau_{m,ca}.$$

Activity coefficient of any species *i* (ion or molecule) can be estimated from the partial derivative of excess Gibbs energy with respect to the number of mole of species *i* using Eq. (24) [7].

$$\ln \gamma_i = \frac{G_m^{*E}}{RT} = \left[ \frac{\delta \left( n G_m^{*E} / RT \right)}{\delta n_i} \right] \quad (24)$$

The above-mentioned electrolyte-NRTL model consists of adjustable non-random factor parameters (*α*) and the binary interaction energy parameters (*τ*). The relationship among the adjustable parameter for any molecule-electrolyte, electrolyte-molecule and electrolyte-electrolyte pair are *α<sub>ij</sub>* = *α<sub>ji</sub>* and *τ<sub>ij</sub>* ≠ *τ<sub>ji</sub>*, (where, *i* and *j* both represent the molecule and electrolyte pair). Interaction between the ion pair – ion pair is often neglected in the electrolyte-NRTL model. Temperature-dependent functions of molecule-molecule binary parameter, molecule-electrolyte pair parameter and electrolyte-molecule pair parameter are shown in Eqs. 25–27.

$$\tau_{m,m} = A_{ij} + \frac{B_{ij}}{T} + E_{ij} \ln(T) + F_{ij}T \quad (25)$$

$$\tau_{m,ca} = C_{m,ca} + \frac{D_{m,ca}}{T} + E_{m,ca} \left[ \frac{(T^{ref} - T)}{T} + \ln \left( \frac{T}{T^{ref}} \right) \right] \quad (26)$$

$$\tau_{ca,m} = C_{ca,m} + \frac{D_{ca,m}}{T} + E_{ca,m} \left[ \frac{(T^{ref} - T)}{T} + \ln \left( \frac{T}{T^{ref}} \right) \right] \quad (27)$$

where, *T<sup>ref</sup>* = 298.15K1

### 3.4. Parameter setting

Several pure components data (pure parameter), data for mixed solvents (binary parameters) and electrolyte-NRTL pair data are necessary to perform the thermodynamic model of CO<sub>2</sub>-amine-water systems. All the necessary pure components data for CO<sub>2</sub> and water and the binary data for CO<sub>2</sub>-water systems already exist in the Aspen Plus databank. Few pure component data of DMAPA

**Table 4**  
Reference state properties used in this model.

|                               | <i>Δ<sub>f</sub>G<sub>i</sub><sup>lg</sup></i> (kJ/kmol) | <i>Δ<sub>f</sub>H<sub>i</sub><sup>lg</sup></i> (kJ/kmol) | <i>Δ<sub>f</sub>G<sub>i</sub><sup>∞</sup></i> (kJ/kmol) | <i>Δ<sub>f</sub>H<sub>i</sub><sup>∞</sup></i> (kJ/kmol) | Source         |
|-------------------------------|--|--|---|---|----------------|
| CO <sub>2</sub>               | −394648  | −393769  | −385980   | −413800   | Aspen databank |
| H <sub>2</sub> O              | −228767  | −241997  |   |   | Aspen databank |
| DMAPA                         | 179700   | −31890   |   |   | Aspen databank |
| H <sup>+</sup>                |  | 1.54E+06   | 0   | 0   | Aspen databank |
| OH <sup>−</sup>               |  | −143510  | −157244   | −229994   | Aspen databank |
| HCO <sub>3</sub> <sup>−</sup> |  |  | −586770   | −691990   | Aspen databank |
| CO <sub>3</sub> <sup>2−</sup> |  |  | −527810   | −677140   | Aspen databank |

were already present in Aspen databank, and few data were taken from the literature. All necessary data to perform this modeling work were already present in the database or were taken from the literature are provided in the following tables. The values of the physical properties of the pure components used in this electrolyte-NRTL model are given in Table 3. Standard properties e.g. standard free energy of formation and standard enthalpy of formation that were used to define the reference state in this study provided in Table 4.

Henry's law constant for CO<sub>2</sub> in water is already available in Aspen databank. The coefficients of the temperature-dependent function of Henry's law constant (Eq. (28)) are provided in Table 5. H<sup>+</sup>DMAPACOO<sup>−</sup> is a charge-neutral component and non-volatile, therefore, a very small Henry's law constant have been assigned [2].

$$\ln H(\text{kPa}) = a + \frac{b}{T(K)} + c \ln T(K) + dT(K) \quad (28)$$

The values of the vapor pressures of CO<sub>2</sub>, H<sub>2</sub>O and DMAPA are available in the Aspen databank as temperature-dependent function as shown in Eq. (29). This is an extended Antoine equation (PLXANT), and the coefficients of this equation for different components used in this model are presented in Table 6. The values of the vapor pressure for all ions associated with CO<sub>2</sub> and H<sub>2</sub>O (H<sup>+</sup>, OH<sup>−</sup>, HCO<sub>3</sub><sup>−</sup> and CO<sub>3</sub><sup>2−</sup>) and other ions associated with DMAPA [5] were taken from the database.

$$\ln p_i^0(\text{kPa}) = C_{1i} + \frac{C_{2i}}{T(K) + C_{3i}} + C_{4i}T(K) + C_{5i} \ln T(K) + C_{6i}T(K)^{C_{7i}} \quad (29)$$

Aspen plus relates the heat of vaporization, the specific heat capacity and the ideal gas enthalpy with Eqs. (30) and (31) [23]; where, *H<sub>i</sub><sup>l</sup>*(*T<sup>ref</sup>*), *H<sub>i</sub><sup>lg</sup>* and *C<sub>p,i</sub><sup>l</sup>* are the reference enthalpy at 298.15 K, the ideal gas enthalpy and liquid heat capacity of component *i*, respectively; and (*H<sub>i</sub><sup>v</sup>* − *H<sub>i</sub><sup>lg</sup>*) is the departure of the vapor enthalpy [23]. The liquid heat capacity and heat of vaporization for H<sub>2</sub>O and DMAPA were already available in the Aspen databank. Coefficients of the temperature-dependent DIPPR equation (Eq. (32)) for estimating heat of vaporization of DMAPA are given in Table 7.

$$H_i^l - H_i^l(T^{ref}) = \int_{T^{ref}}^T C_{p,i}^l dT \quad (30)$$

**Table 5**  
Coefficient of Henry's law constant in H<sub>2</sub>O.

| Solvent         | a       | b        | c        | d        | Source         |
|-----------------|---------|----------|----------|----------|----------------|
| CO <sub>2</sub> | 163.805 | −8477.71 | −21.9574 | 0.005781 | Aspen databank |
| HDMAPACOO       | −10     | 0        | 0        | 0        | This work      |

**Table 6**

Coefficients for Antoine equation (PLXANT) to estimate the vapor pressure.

| Component        | C <sub>1</sub> | C <sub>2</sub> | C <sub>3</sub> | C <sub>4</sub> | C <sub>5</sub> | C <sub>6</sub> | C <sub>7</sub> |
|------------------|----------------|----------------|----------------|----------------|----------------|----------------|----------------|
| H <sub>2</sub> O | 65.6422        | −7206.7        | 0              | 0              | −7.1385        | 4.046E-6       | 2              |
| CO <sub>2</sub>  | 65.9214        | −3403.28       | 0              | 0.009491       | −8.56034       | 2.91E-16       | 6              |
| DMAPA            | 57.9002        | −7163.1        | 0              | 0              | −5.9473        | 7.689E-18      | 6              |
| Ions             | −1.00E+20      | 0              | 0              | 0              | 0              | 0              | 0              |

**Table 7**

Heat of vaporization (kJ/kmol).

| Component | C <sub>1i</sub> | C <sub>2i</sub> | C <sub>3i</sub> | C <sub>4i</sub> | C <sub>5i</sub> | Source         |
|-----------|-----------------|-----------------|-----------------|-----------------|-----------------|----------------|
| DMAPA     | 60583           | 0.65909         | −0.63598        | 0.35445         | 0               | Aspen databank |

$$H_i^l(T^{ref}) = H_i^{ig} + (H_i^v - H_i^{ig}) - \Delta H_i^{vap} \quad (31)$$

$$\Delta_{vap} H_i^* = C_{1i}(1 - T_{ri})^{(C_{2i} + C_{3i}T_{ri} + C_{4i}T_{ri}^2 + C_{5i}T_{ri}^3)} \quad (32)$$

Ideal gas heat capacity and heat capacity in aqueous-phase infinite dilution are very important model parameters, and they are required to estimate standard properties of any molecule and ionic species. The ideal gas heat capacities of the pure components (DMAPA, H<sub>2</sub>O and CO<sub>2</sub>) are already available at the Aspen plus databank as a function of temperature shown in Eq. (33) (Eq. (34) was used for DMAPA). Infinite dilution aqueous phase heat capacity for H<sup>+</sup> and OH<sup>−</sup> are also available at the Aspen plus databank as a function of temperature shown in Eq. (35). However, the heat capacity of HCO<sub>3</sub><sup>−</sup> and CO<sub>3</sub><sup>2−</sup> at infinite dilution were not available. They were taken from Chen et al. (2013) [2]. All the coefficients of the temperature-dependent functions are provided at Table 8.

$$C_{p,i}^{ig} = C_1 + C_2T + C_3T^2 + C_4T^3 + C_5T^4 + C_6T^5 \quad (33)$$

$$C_{p,i}^{ig} = C_1 + C_2 \left( \frac{C_3/T}{\sinh(C_3/T)} \right)^2 + C_4 \left( \frac{C_5/T}{\cosh(C_5/T)} \right)^2 \quad (34)$$

$$C_{p,i}^{\infty,aq} = C_1 + C_2T + C_3T^2 + \frac{C_4}{T} + \frac{C_5}{T^2} + \frac{C_6}{\sqrt{T}} \quad (35)$$

The dielectric constants for all the pure components involved in electrolyte-NRTL model are necessary. Dielectric constants for CO<sub>2</sub> and H<sub>2</sub>O are already available in Aspen databank but the value of the dielectric constant for DMAPA was not available. Functional groups such as OH<sup>−</sup>, COOH<sup>−</sup>, etc. have a significant effect on the value of dielectric constant of the molecule; however, without these functional groups, the values of dielectric constant of various amines with similar structure including primary, secondary or tertiary (e.g. Butylamine, Diethylamine, Pentylamine, Dipropylamine, etc.) are in very close range, and varied from 2.8 to 4.5 at

298.15 K. Due to the unavailability of data, the dielectric constant value of diethylamine was used for this work. Coefficients of temperature-dependent function (Eq. (21)) of the dielectric constant of the molecules are given in Table 9. Eq. (22) is used to estimate the dielectric constant of the mixture from the total combined effect of mass fraction and dielectric constant of the pure component.

NRTL parameters for H<sub>2</sub>O–CO<sub>2</sub> are already available in Aspen databank. NRTL parameters for H<sub>2</sub>O–DMAPA were regressed from the excess enthalpy (H<sup>E</sup>) data and results are shown in Table 10. Few temperature-dependent pair parameters for water-ion pair are already available in Aspen databank (shown in Table 10); and some common CO<sub>2</sub>–ion pair interaction parameters which were used in the models for other CO<sub>2</sub>+amine systems' in the literature [7] were used as default in this study (shown in Table 10). All ion pair – ion pair interaction parameters were neglected in this model. All unregressed water-ion pair interaction parameter ( $\tau_{H_2O-CA}$ ) and ion pair–water interaction parameters ( $\tau_{CA-H_2O}$ ) were set at default values of 8.015 and −4.072, respectively; and all other molecule-ion pair interaction parameters ( $\tau_{molecule-CA}$ ) and ion pair–molecule interaction parameters ( $\tau_{CA-molecule}$ ) were set at default values of 15 and −8, respectively. Nonrandomness factors ( $\alpha$ ) were fixed at 0.2 for water-ion pair parameters, and 0.1 for other molecule-ion pair parameters. All the important molecule-ion pair parameters which were regressed in this study from the experimental VLE data for the tertiary system of DMAPA–H<sub>2</sub>O–CO<sub>2</sub> are provided in Table 10.

### 3.5. Regression of solubility data

Aspen Plus V10 was used to model the vapor-liquid equilibrium (VLE) data. Various thermodynamic parameters were determined by the regression of experimental data with the data regression system (DRS) incorporated in Aspen. The Britt-Luecke algorithm was used for regression to minimize the errors in all measured variables by using the Maximum likelihood objective function shown in Eq. (36) [2,5].

**Table 9**

Coefficients of dielectric constants.

| Molecule         | A <sub>B</sub> | B <sub>B</sub> | C <sub>B</sub> | Source            |
|------------------|----------------|----------------|----------------|-------------------|
| CO <sub>2</sub>  | 1.6            | 0              | 293.15         | Aspen databank    |
| H <sub>2</sub> O | 78.54          | 31989.4        | 298.15         | Aspen databank    |
| DMAPA            | 3.753          | 1532.2         | 298.15         | Used in this work |

**Table 8**Ideal gas heat capacity (C<sub>p,i</sub><sup>ig</sup>, kJ.kmol<sup>−1</sup>.K<sup>−1</sup>) for molecules and infinite dilution aqueous phase heat capacity (C<sub>p,i</sub><sup>∞,aq</sup>, kJ.kmol<sup>−1</sup>.K<sup>−1</sup>) for ions.

|                               | C <sub>1</sub> | C <sub>2</sub> | C <sub>3</sub> | C <sub>4</sub> | C <sub>5</sub> | C <sub>6</sub> | Source                 |
|-------------------------------|----------------|----------------|----------------|----------------|----------------|----------------|------------------------|
| DMAPA                         | 126.14         | 366.91         | 1941.2         | 278.43         | 849.76         |                | Aspen databank         |
| H <sub>2</sub> O              | 33.7381        | −0.00702       | 2.73E-05       | −1.66E-08      | 4.30E-12       | −4.17E-16      | Aspen databank         |
| CO <sub>2</sub>               | 19.7952        | 0.073437       | −5.60E-05      | 1.72E-08       | 0              | 0              | Aspen databank         |
| H <sup>+</sup>                | 0              | 0              | 0              | 0              | 0              | 0              | Aspen databank         |
| OH <sup>−</sup>               | −148.5         | 0              | 0              | 0              | 0              | 0              | Aspen databank         |
| HCO <sub>3</sub> <sup>−</sup> | 211            | −0.882         | 0.000875       | −18800         | 0              | 0              | Chen et al. (2013) [2] |
| CO <sub>3</sub> <sup>2−</sup> | 1330           | −5.56          | 0.00519        | −119000        | 0              | 0              | Chen et al. (2013) [2] |

**Table 10**  
NRTL parameters and pair parameters used in this work.

| Parameter                               | NRTL parameter |          |          |          |          | Ref            |
|---|----------------|----------|----------|----------|----------|----------------|
|   | $A_{12}$       | $A_{21}$ | $B_{12}$ | $B_{21}$ | $\alpha$ |                |
| H <sub>2</sub> O(1)-CO <sub>2</sub> (2) | 10.064         | 10.064   | -3268.14 | -3268.14 | 0.2      | Aspen databank |
| H <sub>2</sub> O(1)-DMAPA(2)            | 16.6874        | -0.0421  | -3790.07 | -785.359 | 0.2      | This study     |

| Parameter                                | Pair parameters |            |            |            |          | Ref                   |
|--|-----------------|------------|------------|------------|----------|-----------------------|
|  | $A_{m,ca}$      | $A_{ca,m}$ | $B_{m,ca}$ | $B_{ca,m}$ | $\alpha$ |                       |
| $\tau_{H_2O-(H^+,OH^-)}$                 | 8.045           | -4.072     | -          | -          | 0.2      | Aspen databank        |
| $\tau_{H_2O-(H^+,HCO_3^-)}$              | 8.045           | -4.072     | -          | -          | 0.2      | Aspen databank        |
| $\tau_{H_2O-(H^+,CO_3^{2-})}$            | 8.045           | -4.072     | -          | -          | 0.2      | Aspen databank        |
| $\tau_{CO_2-(H^+,OH^-)}$                 | 15              | -8         | -          | -          | 0.1      | Liu et al. (1999) [7] |
| $\tau_{CO_2-(H^+,HCO_3^-)}$              | 15              | -8         | -          | -          | 0.1      | Liu et al. (1999) [7] |
| $\tau_{CO_2-(H^+,CO_3^{2-})}$            | 15              | -8         | -          | -          | 0.1      | Liu et al. (1999) [7] |
| $\tau_{H_2O-(DMAPAH^+,HCO_3^-)}$         | 8.88369         | -2.86392   | -          | -          | 0.2      | This study            |
| $\tau_{H_2O-(DMAPAH^+,DMAPACOO^-)}$      | 15.18194        | -5.68643   | -          | -          | 0.2      | This study            |
| $\tau_{H_2O-(DMAPAH^+,CO_3^{2-})}$       | -0.543699       | -          | -          | -          | 0.2      | This study            |
| $\tau_{DMAPA-(DMAPAH^+,HCO_3^-)}$        | -               | -12.8786   | -          | -          | 0.1      | This study            |
| $\tau_{DMAPA-(DMAPAH^+,DMAPACOO^-)}$     | -               | -17.5548   | -          | -          | 0.1      | This study            |
| $\tau_{DMAPA-(DMAPAH^+,CO_3^{2-})}$      | -               | -16.2204   | -          | -          | 0.1      | This study            |
| $\tau_{HDMAPACOO-(DMAPAH^+,HCO_3^-)}$    | -               | -18.6923   | -          | -          | 0.1      | This study            |
| $\tau_{HDMAPACOO-(DMAPAH^+,DMAPACOO^-)}$ | -               | -25.5610   | -          | -          | 0.1      | This study            |
| $\tau_{HDMAPACOO-(DMAPAH^+,CO_3^{2-})}$  | -               | 3.50153    | -          | -          | 0.1      | This study            |
| $\tau_{CO_2-(DMAPAH^+,DMAPACOO^-)}$      | -               | -24.9587   | -          | -          | 0.1      | This study            |

**Table 11**  
Solubility of CO<sub>2</sub> in 15 wt % of DMAPA.

| T = 313.15 K <sup>a</sup> (Run 1) |   | T = 333.15 K <sup>a</sup> (Run 2) |   | T = 333.15 K <sup>a</sup> (Run 3) |   |
|-----------------------------------|---|-----------------------------------|---|-----------------------------------|---|
| $P_{CO_2}$ (kPa) <sup>b</sup>     | $\alpha_{CO_2} \left( = \frac{mol_{CO_2}}{mol_{DMAPA}} \right)^c$ | $P_{CO_2}$ (kPa) <sup>b</sup>     | $\alpha_{CO_2} \left( = \frac{mol_{CO_2}}{mol_{DMAPA}} \right)^c$ | $P_{CO_2}$ (kPa) <sup>b</sup>     | $\alpha_{CO_2} \left( = \frac{mol_{CO_2}}{mol_{DMAPA}} \right)^c$ |
| 0.3                               | 0.418   | 1.2                               | 0.482   | 0.5                               | 0.518   |
| 2.6                               | 0.827   | 15.1                              | 0.939   | 25.3                              | 0.975   |
| 13.6                              | 1.053   | 77.2                              | 1.103   | 100.6                             | 1.114   |
| 55.3                              | 1.201   | 165.8                             | 1.197   | 179.5                             | 1.183   |
| 120.5                             | 1.307   | 234.5                             | 1.254   | 230.2                             | 1.225   |
| 182.9                             | 1.377   | 274.5                             | 1.291   | 260.2                             | 1.252   |
| 230.7                             | 1.421   |                                   |   |                                   |   |
| 271.0                             | 1.456   |                                   |   |                                   |   |

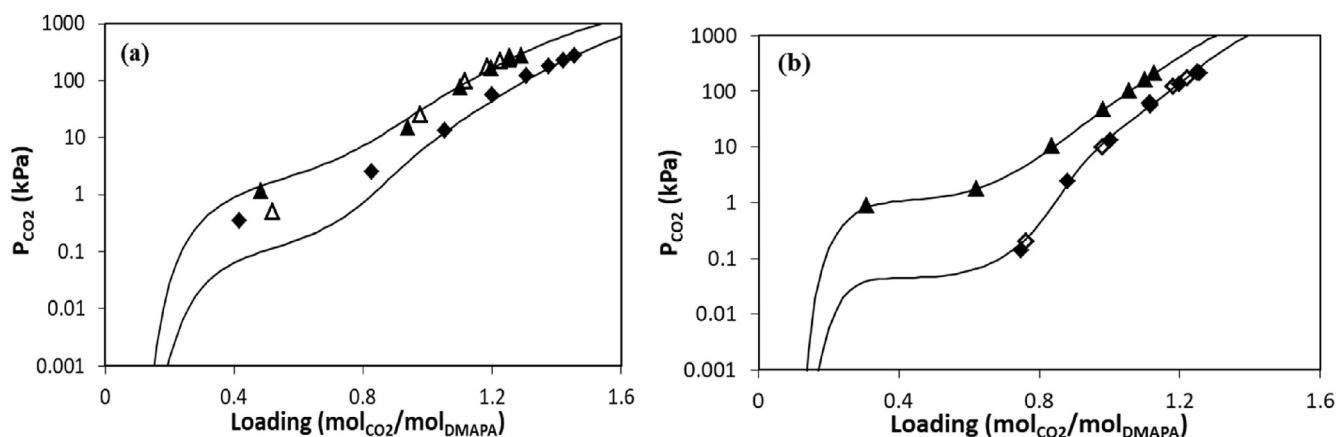
<sup>a</sup> Standard uncertainty  $u(T) = 0.5$  K.  
<sup>b</sup> Standard uncertainty  $u(P) = 0.89$  kPa.  
<sup>c</sup> Standard uncertainty  $u(\alpha_{CO_2}) = 0.107$ .

**Table 12**  
Solubility of CO<sub>2</sub> in 30 wt % of DMAPA.

| T = 313.15 K <sup>a</sup> (Run 4) |   | T = 313.15 K <sup>a</sup> (Run 5) |   | T = 333.15 K <sup>a</sup> (Run 6) |   |
|-----------------------------------|---|-----------------------------------|---|-----------------------------------|---|
| $P_{CO_2}$ (kPa)                  | $\alpha_{CO_2} \left( = \frac{mol_{CO_2}}{mol_{DMAPA}} \right)^c$ | $P_{CO_2}$ (kPa)                  | $\alpha_{CO_2} \left( = \frac{mol_{CO_2}}{mol_{DMAPA}} \right)^c$ | $P_{CO_2}$ (kPa)                  | $\alpha_{CO_2} \left( = \frac{mol_{CO_2}}{mol_{DMAPA}} \right)^c$ |
| 0.2                               | 0.747   | 0.2                               | 0.760   | 0.9                               | 0.307   |
| 2.4                               | 0.881   | 10.2                              | 0.979   | 1.8                               | 0.621   |
| 13.2                              | 1.002   | 60.5                              | 1.114   | 10.5                              | 0.835   |
| 55.2                              | 1.116   | 123.1                             | 1.181   | 47.6                              | 0.980   |
| 131.9                             | 1.199   | 174.6                             | 1.220   | 103.6                             | 1.056   |
| 215.4                             | 1.258   | 222.8                             | 1.250   | 162.4                             | 1.099   |
|                                   |   |                                   |   | 214.1                             | 1.126   |

<sup>a</sup>Standard uncertainty  $u(T) = 0.5$  K.  
<sup>b</sup>Standard uncertainty  $u(P) = 0.89$  kPa.  
<sup>c</sup>Standard uncertainty  $u(\alpha_{CO_2}) = 0.107$ .





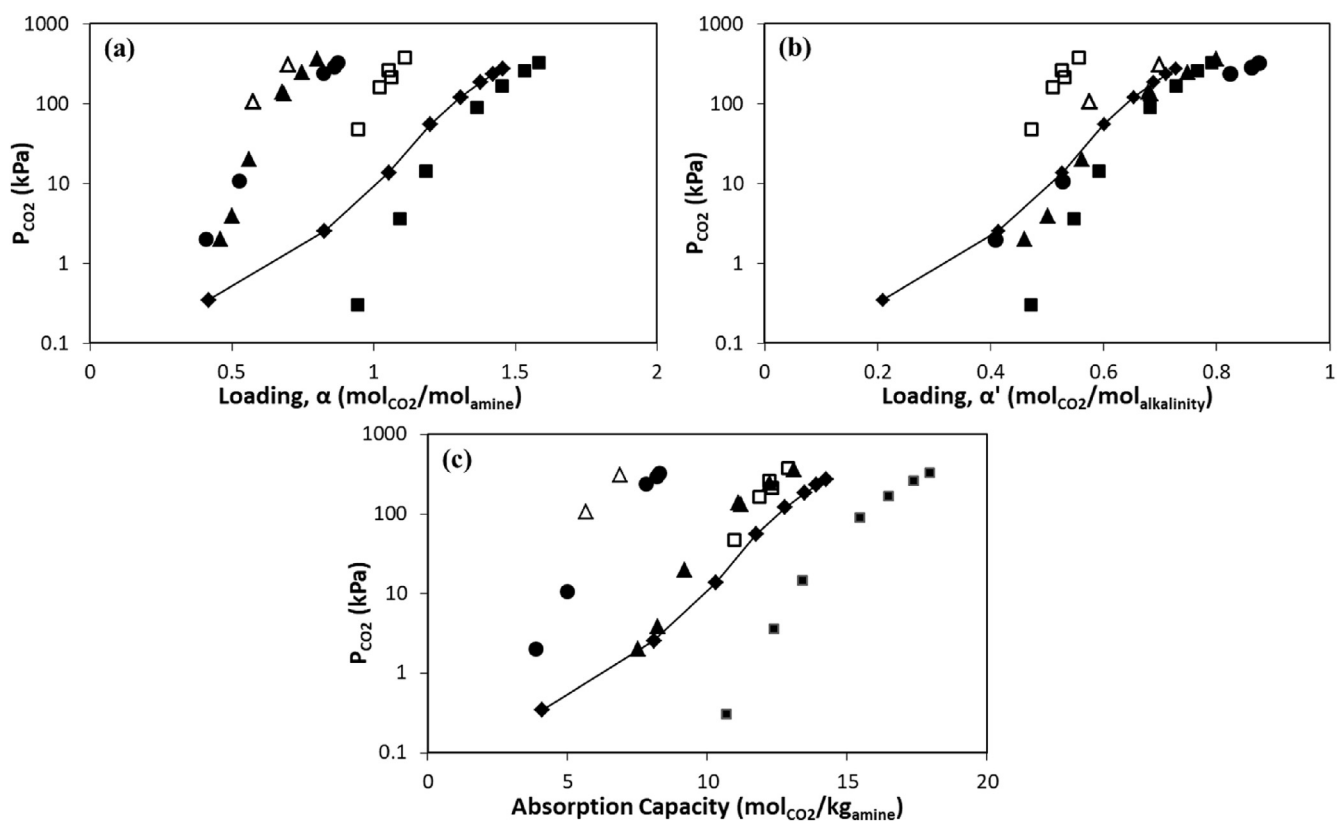
**Fig. 3.** Experimental solubility data of CO<sub>2</sub> in aqueous DMAPA shown with symbol (diamond, 313.15 K and triangle 333.15 K) and data from model correlation shown with line. [Solubility data in 15 wt % and 30 wt % DMAPA shown in (a) (▲: run 2, and Δ: run 3) and (b) (◆: run 4, and ◇: run 5), respectively.

$$OF = \sum_{i=1}^N \left[ \left( \frac{T_i^{est} - T_i^{exp}}{\sigma_{T_i}} \right)^2 + \left( \frac{P_i^{est} - P_i^{exp}}{\sigma_{P_i}} \right)^2 + \left( \frac{x_i^{est} - x_i^{exp}}{\sigma_{x_i}} \right)^2 \right] \quad (36)$$

where, OF is objective function, N is the number of dataset, est and exp are the corresponding estimated and measured variables (temperature, pressure and mole-fraction), and  $\sigma$  is the standard deviation of corresponding measured value.

#### 4. Results and discussion

The solubility of CO<sub>2</sub> in two aqueous solutions of DMAPA, at 15 wt% and 30 wt%, were measured with a pressure decay method, at 313.15 K and 333.15 K, and up-to a partial pressure of CO<sub>2</sub> 275 kPa. All experimental results of the solubility of CO<sub>2</sub> are summarized in Tables 11 and 12, respectively. The experimental loadings (mole of CO<sub>2</sub> absorbed in per mole of DMAPA) at different temperatures and the corresponding equilibrium pressures are also plotted in Fig. 3. Experimental data demonstrate that the partial pressure of CO<sub>2</sub> increases exponentially with loading. At 100 kPa



**Fig. 4.** Comparison of the solubility of CO<sub>2</sub> in aqueous DMAPA with other common amines at 313.15 K. (a) Loading,  $\alpha = \text{mol}_{\text{CO}_2}/\text{mol}_{\text{amine}}$  (b) Loading,  $\alpha' = \text{mol}_{\text{CO}_2}/\text{mol}_{\text{alkalinity}}$  and (c) Absorption Capacity =  $\text{mol}_{\text{CO}_2}/\text{kg-amine}$ . Diamond (◆) with line: 15 wt % DMAPA (this work), ▲: MEA (15 wt %) [19], ●: DEA (25 wt % at 310.92 K) [27], Δ: DIPA (45 wt %) [28], ■: MAPA (17.877 wt %) [29], and □: PZ (10.3 & 17.2 wt %) [30,31].

partial pressure of CO<sub>2</sub>, the loadings of CO<sub>2</sub> in 15 wt % of DMAPA are about 1.303 and 1.144 at 313.15 K and 333.15 K, respectively. These are quite high loadings for such low partial pressures compared to the other common amine-based solvents.

Solubility of CO<sub>2</sub> in 15 wt% aqueous solution of DMAPA estimated in this study was compared with the solubility of CO<sub>2</sub> in other common amines such as monoethanolamine (MEA) [19], diethanolamine (DEA) [27], diisopropanolamine (DIPA) [28], 3-(methylamino)-propylamine (MAPA) [29] and piperazine (PZ) [30,31] in Fig. 4. DMAPA and MAPA exhibited very high loading ( $\alpha = \text{mol}_{\text{CO}_2}/\text{mol}_{\text{amine}}$ ) compared to other amines in Fig. 4a. Since MEA, DEA and DIPA have only one amino group in their structure, while, the others amines are diamines (two amino groups in their structure); therefore, the solubility of CO<sub>2</sub> in amine was also compared in terms of mole of CO<sub>2</sub> absorbed in per mole of amine alkalinity ( $\alpha' = \text{mol}_{\text{CO}_2}/\text{mol}_{\text{alkalinity}}$ ) and mole of CO<sub>2</sub> absorbed in per kilogram (kg) amine. Although DEA showed slightly higher loading ( $\text{mol}_{\text{CO}_2}/\text{mol}_{\text{alkalinity}}$ ) based on alkalinity in Fig. 4b, but DEA demonstrates very low CO<sub>2</sub> loading ( $\text{mol}_{\text{CO}_2}/\text{mol}_{\text{amine}}$ ) in Fig. 4a and low CO<sub>2</sub> absorption capacity ( $\text{mol}_{\text{CO}_2}/\text{kg-amine}$ ) in Fig. 4c. According to this comparison, DMAPA demonstrated a very high CO<sub>2</sub> absorption capacity compared to the other amines except for MAPA. DMAPA exhibited about 1.35 and 1.94 times more CO<sub>2</sub> loading at the same temperature (313.15 K) and pressure (271 kPa) compared to Piperazine and MEA, respectively. In Fig. 5, the solubility of CO<sub>2</sub> in DMAPA was also compared with various piperazine derivatives: piperazine (PZ) [30,31], 1-methyl-piperazine (1MPZ) [32], 1-ethyl piperazine (1EPZ) [32], 1-(2-hydroxyethyl) piperazine (HEP) [32] and 1,4-dimethyl piperazine (DMPZ) [32]. Fig. 5 demonstrated that DMAPA demonstrated higher solubility compared with all the piperazine derivatives.

Excess enthalpy ( $H^E$ ) for the binary DMAPA + H<sub>2</sub>O system was measured using a flow calorimeter at (313.15 and 333.15) K and at 0.5 MPa. Detailed excess enthalpy ( $H^E$ ) data for DMAPA + H<sub>2</sub>O system are reported in Table S2 in the supplementary information section. NRTL parameters for H<sub>2</sub>O-DMAPA were regressed from the excess enthalpy data. Aspen Plus model correlation is compared with the experimental results in Fig. 6.

The model was developed in two stages. In first stage, the NRTL parameters for DMAPA/H<sub>2</sub>O were regressed from the excess enthalpy ( $H^E$ ) data of the DMAPA-water system and equilibrium constants (Eqs. (7) and (8)) for the dissociation DMAPA were regressed from the first and second pK<sub>a</sub> value of DMAPA provided by Tissier and Barillier (1969) [21]. In the second stage the elec-NRTL parameters (molecule-ion pair parameters) and equilibrium

constants for the reactions related to formation DMAPA carbamate and formation of protonated DMAPA carbamate were regressed simultaneously from the VLE data for the tertiary system of DMAPA-H<sub>2</sub>O-CO<sub>2</sub> provided in Tables 11 and 12. The overall %AAD between the experimental value and corresponding estimated value during the regression analysis for total pressure, temperature and mole-fraction of the components were 0.04%, 0.41% and 0.18%, respectively. The regressed value of the equilibrium constants ( $K_4$  and  $K_7$ ) for the reactions shown in Eqs. (6) and (9) are shown in Table 2, and regressed NRTL parameter for H<sub>2</sub>O-DMAPA and the regressed important molecule-ion pair parameters were provided in Table 10. The measured values of temperature (K), pressure (kPa) and mole-fraction from the experiment were compared with the estimated value obtained during the data regression in Fig. 7. The ratios of the experimental pressure to the estimated pressure ( $P_{\text{exp.}}/P_{\text{est.}}$ ) are close to unity, but the ratio of the experimental temperature to the estimated temperature ( $T_{\text{exp.}}/T_{\text{est.}}$ ) and the ratio of the experimental mole-fraction to the estimated mole-fraction ( $x_{\text{exp.}}/x_{\text{est.}}$ ) are little scattered. Fig. 7c shows that the ratios of all the experimental mole-fraction of water to the estimated mole-fraction of water are on the line of unity; whereas, the ratios of experimental mole-fraction to estimated mole-fraction of DMAPA and CO<sub>2</sub> are little scattered. The %AAD of the deviations between experimental mole-fraction and estimated mole-fraction for DMAPA and CO<sub>2</sub> were 0.25% and 0.28%, respectively. Loading and the corresponding partial pressure of CO<sub>2</sub> in 15 wt% and 30 wt% solution of DMAPA at the temperatures 313.15 K and 333.15 K were

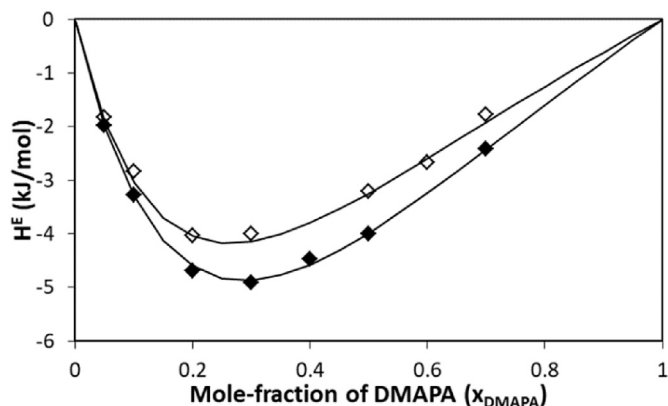


Fig. 6. Excess enthalpy ( $H^E$ ) for the binary DMAPA + H<sub>2</sub>O system: 313.15 K (◆), 333.15 K (◇) and Aspen Plus model prediction (lines).

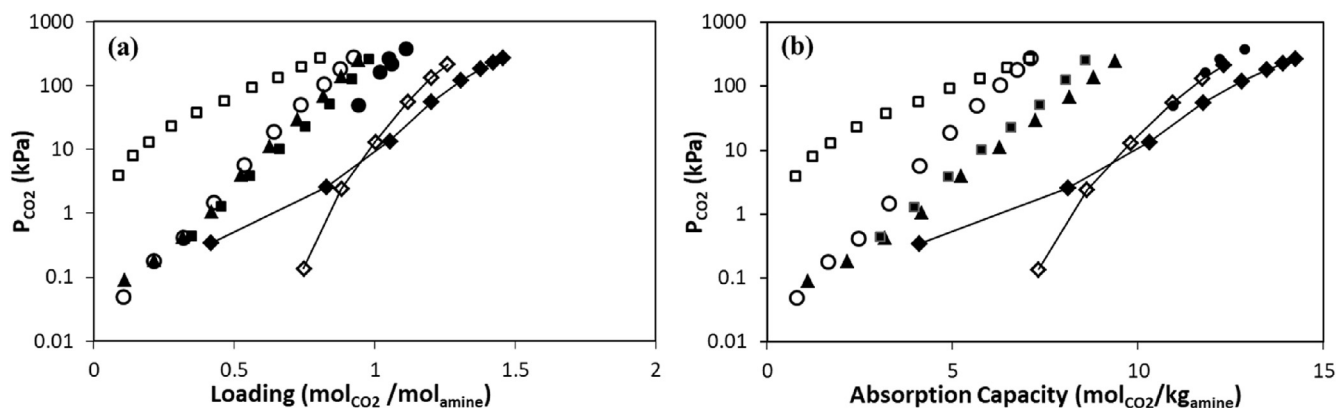
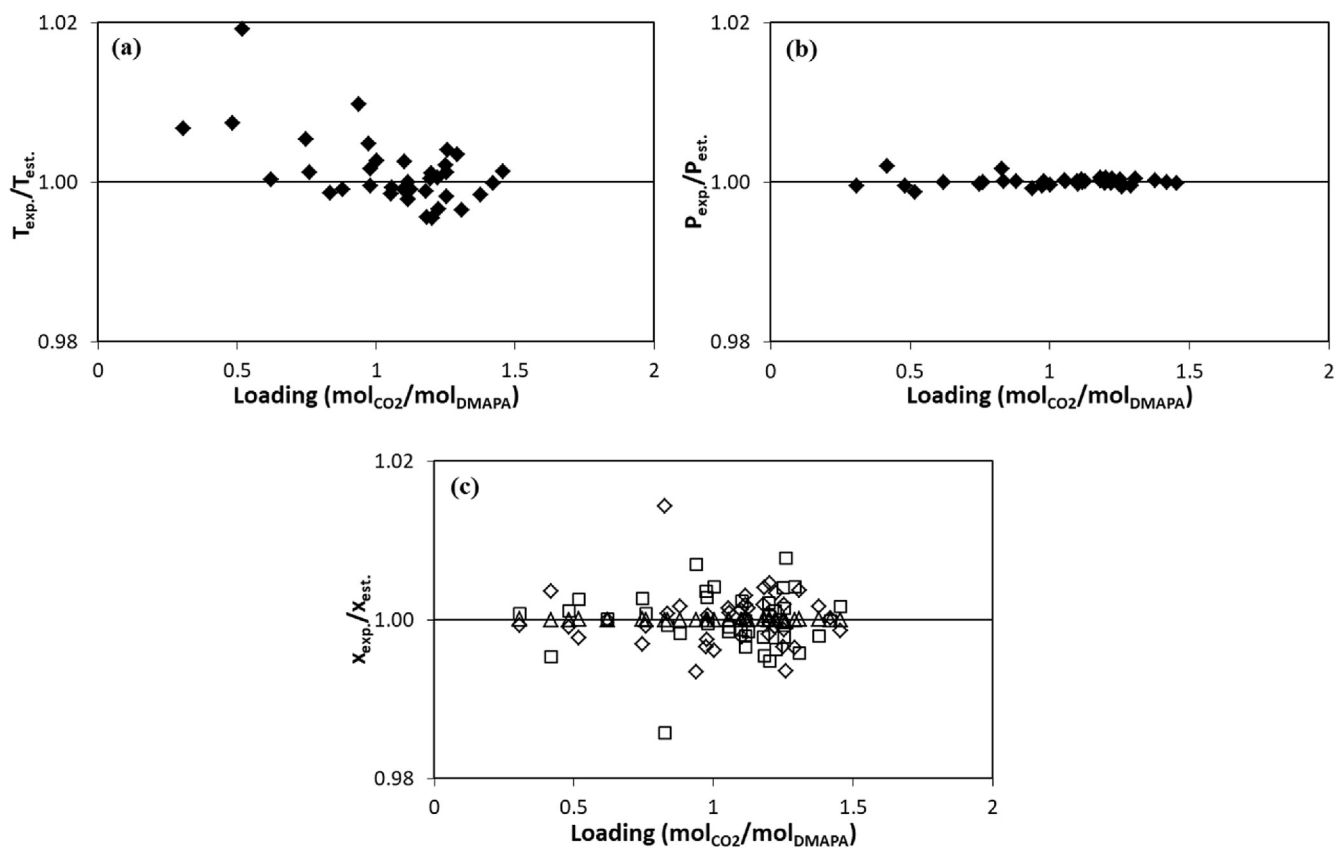
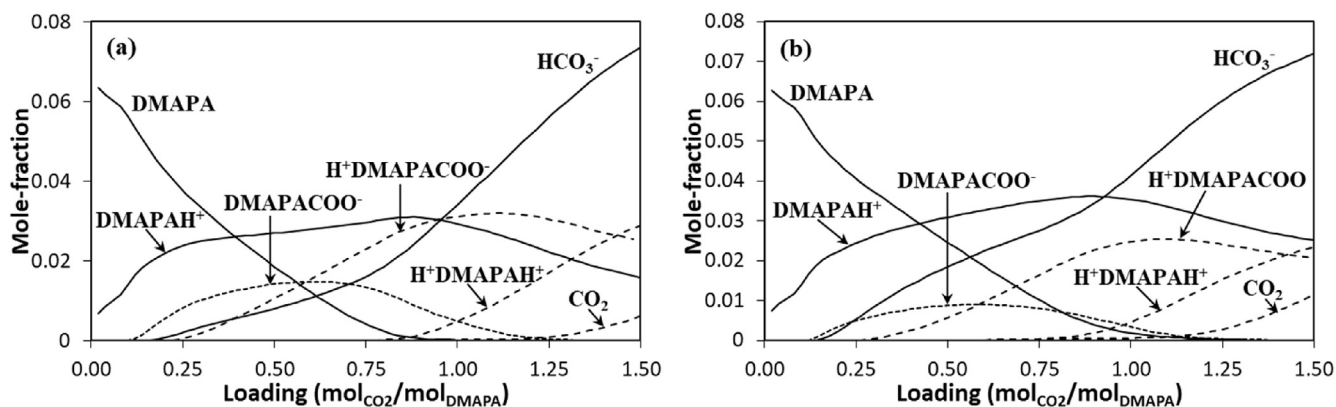


Fig. 5. Comparison of the solubility of CO<sub>2</sub> in DMAPA with the solubility of CO<sub>2</sub> in piperazine derivatives at 313.15 K. (a) Loading,  $\alpha' = \text{mol}_{\text{CO}_2}/\text{mol}_{\text{alkalinity}}$  and (b) Absorption Capacity =  $\text{mol}_{\text{CO}_2}/\text{kg}_{\text{amine}}$ . Diamond: DMAPA (◆: 15 wt % and ◇: 30 wt %), ●: PZ (10.3 & 17.2 wt %) [30,31], ▲: 1MPZ (30 wt %) [32], ■: 1EPZ (30 wt %) [32], ○: HEP (30 wt %) [32] and □: DMPZ (30 wt %) [32].



**Fig. 7.** Comparison among the measured values from experiment and estimated values during regression analysis over various CO<sub>2</sub> loadings. (a) Experimental temperature (K) and estimated temperature (K), (b) experimental pressure (kPa) and estimated temperature (kPa), and (c) experimental mole-fraction and estimated mole-fraction ( $\diamond$ :  $x_{\text{DMAPA,exp.}}/x_{\text{DMAPA,est.}}$ ,  $\square$ :  $x_{\text{CO}_2,\text{exp.}}/x_{\text{CO}_2,\text{est.}}$ , and  $\Delta$ :  $x_{\text{H}_2\text{O,exp.}}/x_{\text{H}_2\text{O,est.}}$ ).



**Fig. 8.** Predicted liquid-phase speciation in 30 wt% DMAPA solution over CO<sub>2</sub> loadings from 0 to 1.5: (a) at 313.15 K and (b) at 333.15 K.

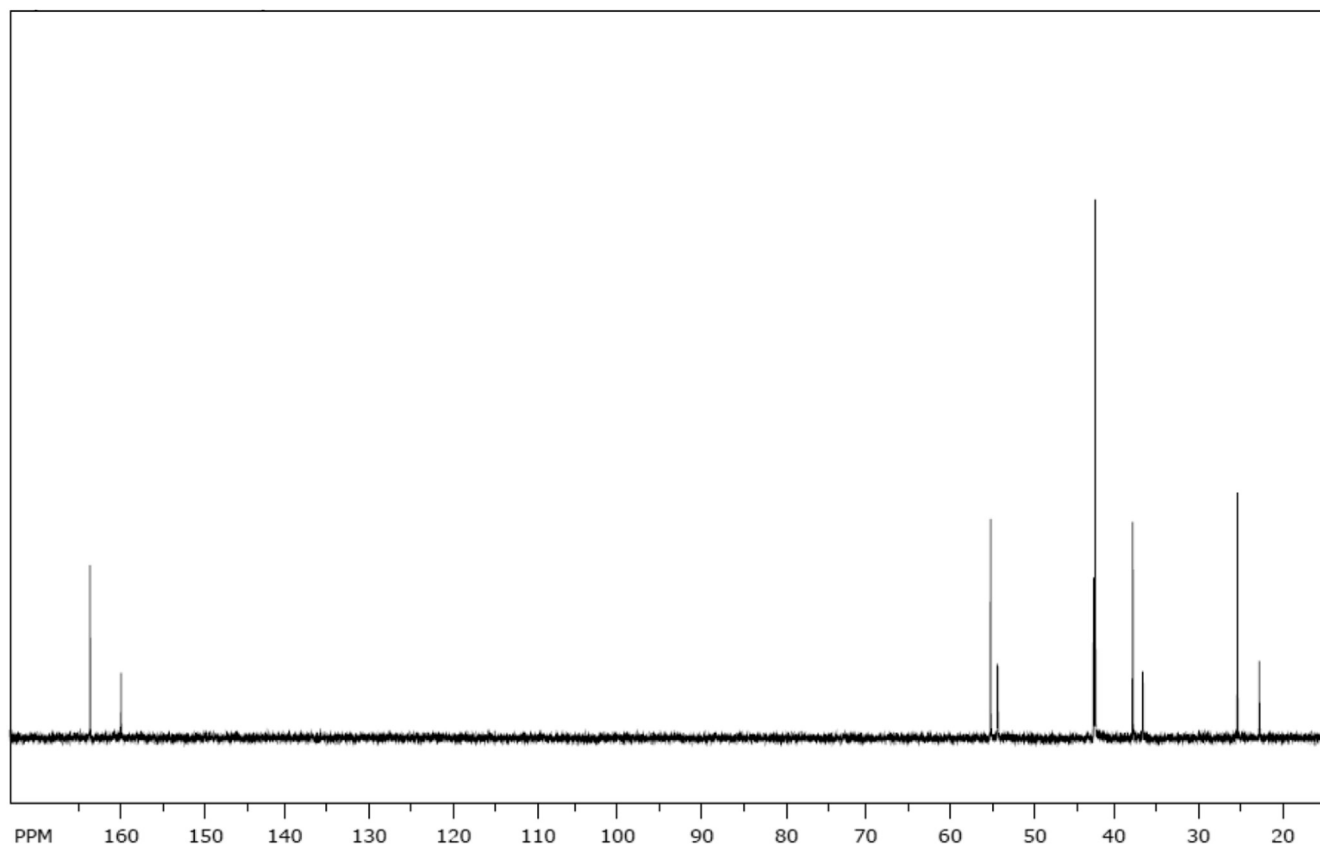
predicted using the model and compared with the experimental results in Fig. 3.

Plot of the speciation concentration can be used to analyze the simulation results of absorber design for CO<sub>2</sub> capture [7]. Concentrations of key species in the liquid phase were predicted with the electrolyte-NRTL model; and the variations of key species in the liquid phase with the CO<sub>2</sub> loading from 0 to 1.5 in 30 wt % aqueous solution of DMAPA at (313.15 and 333.15) K were shown in Fig. 8. Trends for the concentration changes of key species such as DMAPA, carbamate (DMAPACOO<sup>-</sup>), HCO<sub>3</sub><sup>-</sup>, etc. were found similar to the other CO<sub>2</sub>-amine systems [2,7,33,34]. Fig. 8 shows that the concentration of DMAPA decreases with CO<sub>2</sub> loading, and

it almost diminished after the CO<sub>2</sub> loading of 1.0. From Fig. 8, we can infer that major key species in the liquid phase are DMAPACOO<sup>-</sup>, H<sup>+</sup>DMAPACOO<sup>-</sup>, HCO<sub>3</sub><sup>-</sup>, DMAPAH<sup>+</sup> and H<sup>+</sup>DMAPAH<sup>+</sup>. The concentration of DMAPACOO<sup>-</sup> increases with the incremental increase of CO<sub>2</sub> loading at the beginning, and then the concentration starts to decline after a certain loading of CO<sub>2</sub> (around 0.6); whereas, the concentration of H<sup>+</sup>DMAPACOO<sup>-</sup> was very low at the beginning compared to DMAPACOO<sup>-</sup>; however, the concentration of H<sup>+</sup>DMAPACOO<sup>-</sup> increased with the CO<sub>2</sub> loading and it crossed the concentration of DMAPACOO<sup>-</sup> at certain loading. The concentration of HCO<sub>3</sub><sup>-</sup> increased over the range of CO<sub>2</sub> loading between 0 and 1.5; however, the

**Table 13**  
Summary of  $^{13}\text{C}$  NMR spectroscopy for  $\text{CO}_2$  loaded 15 wt% and 30 wt% DMAPA.

| 15 wt% DMAPA   |   |
|----------------|---|
| $\delta$ (ppm) | Species   |
| 22.384         | Second Carbon from primary amino group of DMAPA/protonated-DMAPA                |
| 25.086         | Second Carbon from primary amino group of carbamate/protonated-carbamate        |
| 36.564         | Carbon next to primary amino group of DMAPA/protonated-DMAPA                    |
| 37.671         | Carbon next to primary amino group of carbamate/protonated-carbamate            |
| 42.396         | Methyl carbon next to tertiary amino group of DMAPA/protonated-DMAPA            |
| 54.206         | Methylene carbon next to tertiary amino group of DMAPA/protonated-DMAPA         |
| 55.089         | Methylene carbon next to tertiary amino group of carbamate/protonated-carbamate |
| 160.265        | Carbon of carbonate/bicarbonate species   |
| 164.257        | Carbamate Carbon of carbamate/protonated-carbamate                              |
| 30 wt% DMAPA   |   |
| $\delta$ (ppm) | Species   |
| 22.432         | Second Carbon from primary amino group of DMAPA/protonated-DMAPA                |
| 25.096         | Second Carbon from primary amino group of carbamate/protonated-carbamate        |
| 36.558         | Carbon next to primary amino group of DMAPA/protonated-DMAPA                    |
| 37.776         | Carbon next to primary amino group of carbamate/protonated-carbamate            |
| 42.319         | Methyl carbon next to tertiary amino group of DMAPA/protonated-DMAPA            |
| 54.125         | Methylene carbon next to tertiary amino group of DMAPA/protonated-DMAPA         |
| 54.978         | Methylene carbon next to tertiary amino group of carbamate/protonated-carbamate |
| 160.311        | Carbamate Carbon of carbonate/bicarbonate species                               |
| 164.054        | Carbamate Carbon of carbamate/protonated-carbamate                              |

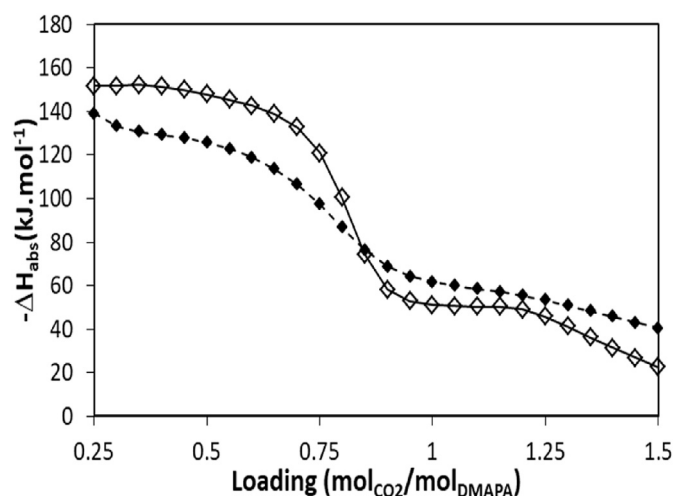


**Fig. 9.**  $^{13}\text{C}$  NMR spectroscopy for  $\text{CO}_2$  loaded 30 wt% DMAPA.

concentration was very low up to 0.15 in loading. The concentration of  $\text{CO}_2$  was insignificant at the beginning, but increased significantly after the  $\text{CO}_2$  loading of 1.25.

Carbamate formation of aqueous DMAPA solution was monitored with  $^{13}\text{C}$  NMR spectroscopy. NMR spectroscopy of  $\text{CO}_2$  loaded 15 wt% and 30 wt% DMAPA solution was obtained with Varian INOVA LC-500MHz NMR spectrometer.  $\text{CO}_2$  was bubbled into aqueous

DMAPA solutions about an hour at room temperature to perform NMR spectroscopy to observe the carbamate formation.  $^{13}\text{C}$  NMR spectroscopy provided the information of carbamate DMAPA, unreacted DMAPA and other species such as bicarbonate and carbonate. Summary for  $^{13}\text{C}$  NMR spectroscopy is provided in Table 13. Chemical shifts of various species including DMAPA/protonated-DMAPA, carbamate/protonated-carbamate and bicarbonate/



**Fig. 10.** Predicted heat of absorptions of CO<sub>2</sub> in aqueous DMAPA solution at 313.15 K (◆: 15 wt% DMAPA and ◊: 30 wt% DMAPA).

carbonate are provided in ppm. Peak location of various species in 15 wt% and 30 wt% DMAPA solution were very close. A sample spectrum acquired for CO<sub>2</sub> loaded 30 wt% DMAPA is shown in Fig. 9.

The heat of absorption of CO<sub>2</sub> in 15 wt% and 30 wt% of DMAPA was estimated using the Gibbs-Helmholtz equation (Eq. (37)). Fugacities of CO<sub>2</sub> for various loadings were predicted at various temperatures using this model with the regressed parameters. The natural log of the CO<sub>2</sub> fugacities for each loading were plotted against the inverse temperatures to predict the heat of absorption, while the changes in temperature are very small (0.1 K) [2]. The Predicted heat of absorption values are presented in Fig. 10.

$$\frac{\Delta H_{abs}}{R} = \left[ \frac{d \ln f_{CO_2}}{d(1/T)} \right]_{\alpha_{CO_2}} \quad (37)$$

The predicted heat of absorption of CO<sub>2</sub> in aqueous DMAPA solution using the Gibbs Helmholtz equation is higher compared with bench-marked amines such as mono-ethanolamine (MEA) and piperazine (PZ). Estimated heat of absorption using calorimeter for CO<sub>2</sub> in 30 wt% MEA and 6.9 wt% PZ for zero loading (as the loading approaches to zero) at 313.15 K are around 85 kJ/mol-CO<sub>2</sub> and 73 kJ/mol-CO<sub>2</sub> [35], respectively; and heat of absorption for CO<sub>2</sub> in 19 wt% PZ for zero loading at 318.15 K is around 92 kJ/mol-CO<sub>2</sub> [36]. However, the predicted heat of absorption from the Gibbs Helmholtz equation may have uncertainties ranging between 20 and 30% when the solubility data is accurate to 2–3% [5,37].

## 5. Conclusion

The solubility of CO<sub>2</sub> in aqueous DMAPA was measured at (313.15 and 333.15) K and at partial pressures of CO<sub>2</sub> up to 275 kPa using the pressure-decay method. In the present study, CO<sub>2</sub> solubility was measured at two aqueous concentrations of DMAPA (15 wt % and 30 wt %) at both temperatures. DMAPA exhibited high CO<sub>2</sub> loading compared with other bench-marked amines such as MEA and Piperazine. Excess enthalpies (H<sup>E</sup>) for the DMAPA-water binary systems were measured using a C80 flow calorimeter at (313.15 and 333.15) K. Finally, the experimental solubility data were correlated with the electrolyte-NRTL model, and the Redlich-Kwong (RK) equation of state was used for the estimation of vapor phase fugacity coefficients at equilibrium. The heats of absorption of CO<sub>2</sub> in 15 wt% and 30 wt% of DMAPA was predicted with the Gibbs-Helmholtz at 313.15 K. The experimental solubility data would qualify DMAPA as a promising solvent for CO<sub>2</sub> removal from flue gas.

## Declaration of competing interest

The authors declare that they have no known competing financial interests or personal relationships that could have appeared to influence the work reported in this paper.

## CRediT authorship contribution statement

**Amr Henni:** Conceptualization, Resources, Supervision, Project administration, Writing - review & editing, Funding acquisition.

## Acknowledgements

The authors would like to acknowledge research funding from the Natural Sciences and Engineering Research Council of Canada (Discovery Grants Program).

## Appendix A. Supplementary data

Supplementary data to this article can be found online at <https://doi.org/10.1016/j.fluid.2020.112506>.

## References

- [1] L. Peter Siegmund, P.C. (CSIRO author (Royal N.M.I.J.A. (University of G.A. Omar Baddour (WMO), C.N. d'Etudes C.S.C.A. Ancy Cazenave (Laboratoire d'Etudes en Géophysique et Océanographie Spatiales, A.G. (Météo-F.S. and O.M.-P.F. Chris Derksen (Environment and Climate Change Canada), J.K. (UK S.H. (Environment and C.C.C.M.H. (ETH Z. Kirsten Isensee (IOC-UNESCO), S.R. (Food and A.O. of M.O.R.M. (Danish M.I. Rodica Nitu (WMO), B.T. (Bureau of M. the U.N.K.S. (IOC-U.M.S. (WMO) Oksana Tarasova (WMO), M.Z. (Deutscher W. Australia), The Global Climate in 2015–2019, World Meteorological Organization, Geneva, Switzerland, 2019. [https://library.wmo.int/index.php?lvl=notice\\_display&id=21522#XflvEPx7mM8](https://library.wmo.int/index.php?lvl=notice_display&id=21522#XflvEPx7mM8).
- [2] X. Chen, G.T. Rochelle, Thermodynamics of CO<sub>2</sub>-2-methylpiperazine/water, Ind. Eng. Chem. Res. 52 (2013) 4229–4238, <https://doi.org/10.1021/ie3023725>.
- [3] S.A. Freeman, R. Dugas, D. Van Wagener, T. Nguyen, G.T. Rochelle, Carbon dioxide capture with concentrated, aqueous piperazine, Energy Procedia 1 (2009) 1489–1496, <https://doi.org/10.1016/j.egypro.2009.01.195>.
- [4] N.A. Fine, P.T. Nielsen, G.T. Rochelle, Decomposition of nitrosamines in CO<sub>2</sub> capture by aqueous piperazine or monoethanolamine, Environ. Sci. Technol. 48 (2014) 5996–6002, <https://doi.org/10.1021/es404949v>.
- [5] A.V. Rayer, Y. Armugam, A. Henni, P. Tontiwachwuthikul, High-pressure solubility of carbon dioxide (CO<sub>2</sub>) in AQUEOUS 1-methyl piperazine solution, J. Chem. Eng. Data 59 (2014) 3610–3623, <https://doi.org/10.1021/je500526m>.
- [6] A.V. rayer, K.Z. sumon, A. Henni, P. Tontiwachwuthikul, Kinetics of the reaction of carbon dioxide (CO<sub>2</sub>) with cyclic amines using the stopped-flow technique, Energy Procedia 4 (2011) 140–147, <https://doi.org/10.1016/j.egypro.2011.01.034>.
- [7] Y. Liu, L. Zhang, S. Watanasiri, Representing Vapor–Liquid equilibrium for an aqueous MEA–CO<sub>2</sub> system using the electrolyte nonrandom-two-liquid model, Ind. Eng. Chem. Res. 38 (5) (1999) 2080–2090, <https://doi.org/10.1021/ie980600v>.
- [8] R.H. Weiland, T. Chakravarty, A.E. Mather, Solubility of carbon dioxide and hydrogen sulfide in aqueous alkanolamines, Ind. Eng. Chem. Res. 32 (1993) 1419–1430, <https://doi.org/10.1021/ie00019a016>.
- [9] C.-C. Chen, L.B. Evans, A local composition model for the excess Gibbs energy of aqueous electrolyte systems, AIChE J. 32 (1986) 444–454, <https://doi.org/10.1002/aic.690320311>.
- [10] F.A. Chowdhury, H. Yamada, T. Higashii, K. Goto, M. Onoda, CO<sub>2</sub> capture by tertiary amine absorbents: a performance comparison study, Ind. Eng. Chem. Res. 52 (2013) 8323–8331, <https://doi.org/10.1021/ie400825u>.
- [11] N. El Hadri, D.V. Quang, E.L.V. Goetheer, M.R.M. Abu Zahra, Aqueous amine solution characterization for post-combustion CO<sub>2</sub> capture process, Appl. Energy 185 (2017) 1433–1449, <https://doi.org/10.1016/j.apenergy.2016.03.043>.
- [12] R. Zhang, Q. Yang, B. Yu, H. Yu, Z. Liang, Toward to efficient CO<sub>2</sub> capture solvent design by analyzing the effect of substituent type connected to N-atom, Energy 144 (2018) 1064–1072, <https://doi.org/10.1016/j.energy.2017.12.095>.
- [13] A. Cachaza, D. Gómez-Díaz, A. Montáns, J.M. Navaza, A. Rumbo, Carbon dioxide chemical absorption by solvents based on diamine and amines blend, AIChE J. 64 (2018) 2702–2710, <https://doi.org/10.1002/aic.16137>.
- [14] M.R. Bohloul, A. Vatani, S.M. Peyghambarzadeh, Experimental and theoretical study of CO<sub>2</sub> solubility in N-methyl-2-pyrrolidone (NMP), Fluid Phase Equil. 365 (2014) 106–111, <https://doi.org/10.1016/j.fluid.2013.12.019>.



- [15] M.M. Taib, T. Murugesan, Solubilities of CO<sub>2</sub> in aqueous solutions of ionic liquids (ILs) and monoethanolamine (MEA) at pressures from 100 to 1600 kPa, *Chem. Eng. J.* 181–182 (2012) 56–62, <https://doi.org/10.1016/j.cej.2011.09.048>.
- [16] C. Mathonat, V. Hynek, V. Majer, J.-P.E. Grolier, Measurements of excess enthalpies at high temperature and pressure using a new type of mixing unit, *J. Solut. Chem.* 23 (1994) 1161–1182, <https://doi.org/10.1007/BF00974028>.
- [17] A.V. Rayer, A. Henni, Heats of absorption of CO<sub>2</sub> in aqueous solutions of tertiary amines: N-methyldiethanolamine, 3-Dimethylamino-1-propanol, and 1-Dimethylamino-2-propanol, *Ind. Eng. Chem. Res.* 53 (2014) 4953–4965, <https://doi.org/10.1021/ie4041324>.
- [18] K.P. Shen, M.H. Li, Solubility of carbon dioxide in aqueous mixtures of monoethanolamine with methyldiethanolamine, *J. Chem. Eng. Data* 37 (1992) 96–100, <https://doi.org/10.1021/je00005a025>.
- [19] J.I. Lee, F.D. Otto, A.E. Mather, The solubility of H<sub>2</sub>S and CO<sub>2</sub> in aqueous monoethanolamine solutions, *Can. J. Chem. Eng.* 52 (1974) 803–805, <https://doi.org/10.1002/cjce.5450520617>.
- [20] J.I. Lee, F.D. Otto, A.E. Mather, Equilibrium between carbon dioxide and aqueous monoethanolamine solutions, *J. Appl. Chem. Biotechnol.* 26 (1) (1976) 541–549, <https://doi.org/10.1002/jctb.5020260177>.
- [21] C. Tissier, P. Barillie, Acidity constants and thermodynamic functions of acids conjugated with some propanediamines, *C. R. Hebd. Seances Acad. Sci. Ser. C* 268 (1969) 1953.
- [22] H. Li, P.T. Frailie, G.T. Rochelle, J. Chen, Thermodynamic modeling of piperazine/2-aminomethylpropanol/CO<sub>2</sub>/water, *Chem. Eng. Sci.* 117 (2014) 331–341, <https://doi.org/10.1016/j.ces.2014.06.026>.
- [23] M.D. Hilliard, A Predictive Thermodynamic Model for an Aqueous Blend of Potassium Carbonate, Piperazine, and Monoethanolamine for Carbon Dioxide Capture from Flue Gas, 2008, p. 1061. <https://repositories.lib.utexas.edu/handle/2152/3900>.
- [24] G. Soave, Equilibrium constants from a modified Redlich-Kwong equation of state, *Chem. Eng. Sci.* 27 (1972) 1197–1203, [https://doi.org/10.1016/0009-2509\(72\)80096-4](https://doi.org/10.1016/0009-2509(72)80096-4).
- [25] O. Redlich, J.N.S. Kwong, On the thermodynamics of solutions. V. An equation of state. Fugacities of gaseous solutions, *Chem. Rev.* 44 (1949) 233–244, <https://doi.org/10.1021/cr60137a013>.
- [26] C.-C. Chen, Y. Song, Generalized electrolyte-NRTL model for mixed-solvent electrolyte systems, *AIChE J.* 50 (2004) 1928–1941, <https://doi.org/10.1002/aic.10151>.
- [27] J.D. Lawson, A.W. Garst, Gas sweetening data: equilibrium solubility of hydrogen sulfide and carbon dioxide in aqueous monoethanolamine and aqueous diethanolamine solutions, *J. Chem. Eng. Data* 21 (1976) 20–30, <https://doi.org/10.1021/je60068a010>.
- [28] A. Haghtalab, H. Eghbali, A. Shojaeian, Experiment and modeling solubility of CO<sub>2</sub> in aqueous solutions of Diisopropanolamine + 2-amino-2-methyl-1-propanol + Piperazine at high pressures, *J. Chem. Thermodyn.* 71 (2014) 71–83, <https://doi.org/10.1016/j.jct.2013.11.025>.
- [29] M.W. Arshad, H.F. Svendsen, P.L. Fosbøl, N. Von Solms, K. Thomsen, Equilibrium total pressure and CO<sub>2</sub> solubility in binary and ternary aqueous solutions of 2-(Diethylamino)ethanol (DEEA) and 3-(Methylamino)propylamine (MAPA), *J. Chem. Eng. Data* 59 (2014) 764–774, <https://doi.org/10.1021/je400886w>.
- [30] S. Kadiwala, A.V. Rayer, A. Henni, High pressure solubility of carbon dioxide (CO<sub>2</sub>) in aqueous piperazine solutions, *Fluid Phase Equil.* 292 (2010) 20–28, <https://doi.org/10.1016/j.fluid.2010.01.009>.
- [31] V. Ermatchkov, A. Pérez-Salado Kamps, D. Speyer, G. Maurer, Solubility of carbon dioxide in aqueous solutions of piperazine in the low gas loading region, *J. Chem. Eng. Data* 51 (2006) 1788–1796, <https://doi.org/10.1021/je0601917>.
- [32] H. Li, Y. Le Moulec, J. Lu, J. Chen, J.C.V. Marcos, G. Chen, Solubility and energy analysis for CO<sub>2</sub> absorption in piperazine derivatives and their mixtures, *Int. J. Greenh. Gas Contr.* 31 (2014) 25–32, <https://doi.org/10.1016/j.ijggc.2014.09.012>.
- [33] S. Bishnoi, G.T. Rochelle, Thermodynamics of piperazine/methyldiethanolamine/water/carbon dioxide, *Ind. Eng. Chem. Res.* 41 (2002) 604–612, <https://doi.org/10.1021/ie0103106>.
- [34] H. Li, Y. Le Moulec, J. Lu, J. Chen, J.C. Valle Marcos, G. Chen, F. Chopin, CO<sub>2</sub> solubility measurement and thermodynamic modeling for 1-methylpiperazine/water/CO<sub>2</sub>, *Fluid Phase Equil.* 394 (2015) 118–128, <https://doi.org/10.1016/j.fluid.2015.03.021>.
- [35] J. Liu, S. Wang, H.F. Svendsen, M.U. Idrees, I. Kim, C. Chen, Heat of absorption of CO<sub>2</sub> in aqueous ammonia, piperazine solutions and their mixtures, *Int. J. Greenh. Gas Contr.* 9 (2012) 148–159, <https://doi.org/10.1016/j.ijggc.2012.03.013>.
- [36] H. Svensson, C. Hultberg, H.T. Karlsson, Heat of absorption of CO<sub>2</sub> in aqueous solutions of N-methyldiethanolamine and piperazine, *Int. J. Greenh. Gas Contr.* 17 (2013) 89–98, <https://doi.org/10.1016/j.ijggc.2013.04.021>.
- [37] I. Kim, H.F. Svendsen, Heat of absorption of carbon dioxide (CO<sub>2</sub>) in monoethanolamine (MEA) and 2-(aminoethyl)ethanolamine (AEEA) solutions, *Ind. Eng. Chem. Res.* 46 (2007) 5803–5809, <https://doi.org/10.1021/ie0616489>.